

Heat-Flux Gauge Studies of Compressible Dynamic Stall

M. S. Chandrasekhara*

Naval Postgraduate School, Monterey, California 93943

and

M. C. Wilder†

NASA Ames Research Center, Moffett Field, California 94035-1000

Compressible dynamic stall was studied using 148 closely spaced heat-flux gauges distributed over the surface of an oscillating, 15.24-cm chord NACA 0012 airfoil. The study has revealed the various surface flow features of compressible dynamic stall. These include the rapid movement of the transition onset point over the airfoil upper surface on the upstroke with increasing angle of attack, the signature of the convecting dynamic-stall vortex, and the relaminarization of the reattaching shear layer on the downstroke. The imprint of a leading-edge shock has been captured for the first time in the surface flow signature. Even though compressible dynamic stall can originate from several causes depending upon flow conditions, the study led to the conclusion that a deterministic precursor of dynamic-stall onset is a sharp rise in the surface shear stress in the leading-edge adverse pressure gradient region, which is a common and singular flow feature at all conditions tested.

Introduction

A FUNDAMENTAL understanding of dynamic-stall onset is important to both rotary- and fixed-wing aerodynamicists. Dynamic stall refers to the stall process of an airfoil executing an unsteady change in angle of attack, for example, sinusoidal pitch oscillations. During such a motion, the airfoil can reach angles of attack exceeding the static-stall angle and generate lift in excess of the maximum static lift. The process culminates in the formation of a dynamic-stall vortex, which propagates along the chord of the airfoil producing large variations in the pitching moment. These pitching-moment variations associated with the dynamic-stall vortex can lead to excessive vibratory loads on aircraft components, such as helicopter pitch links and rotor blades. As a consequence, the large dynamic lift developed prior to the onset of dynamic stall has remained unexploited. A thorough understanding of the mechanism of dynamic-stall vortex formation is necessary for developing a practical control system.

The global flow for an oscillating NACA 0012 airfoil was extensively documented in previous studies¹ using point diffraction interferometry (PDI). It was shown in Ref. 1 that in the compressible regime dynamic stall arises from a variety of onset mechanisms that depend subtly on the global flow conditions (e.g., Mach and Reynolds numbers). A measurement technique like PDI, however, is incapable of resolving the surface-flow details at the scale of the leading-edge boundary layer ($\approx 250 \mu\text{m}$) where dynamic stall originates. It is clear too that particle-based optical techniques are not satisfactory for surface measurements because of incidental problems (glare, reflection, and spatial resolution). In addition, these techniques suffer from particle lag effects, which are amplified near the wall region because of the very large flow gradients present. Therefore, it was decided to use very thin heat-flux gauges for sensing the surface flow. Although there is no known calibration method

available for the measurement of skin friction in adverse-pressure-gradient-driven unsteady flows, the variation of surface heat flux, throughout the oscillation cycle and at various chordwise locations, provides valuable qualitative data that can be appropriately interpreted. Furthermore, the existing global flow measurements can be used to corroborate the interpretation of the results obtained with the heat-flux gauges.

Oscillating airfoil flows have been studied in the past using multiple heat-flux gauges,²⁻⁵ and the fundamentals involved in interpreting the heat-flux gauge data in steady flow have been described by Nakayama et al.⁶ and Stack et al.⁷ The latter group pioneered the use of this technique and the fabrication of the sensors. All of these studies have focused on low-speed flows. They have also been only qualitative because calibration to determine the skin friction is a challenge, as already mentioned. Despite this limitation, analyzing the sensor output traces can generate significant physical insight into the flow. In all of these studies, even though many sensors were used, the distribution of the sensors over the surface can still be deemed sparse. They were also limited to certain regions of the flow. In the previous studies of dynamic-stall flow, the heat-flux gauges covered only the leading few percent of chord.

This study primarily considers unsteady compressible flow, and compressible dynamic stall in particular, and has documented the various underlying flow events. A very large number of sensors were used, covering the entire upper surface and some of the lower surface, as described in the next section.

Description of the Experiment

The tests were conducted at Mach numbers ranging from 0.2 to 0.45 and at reduced frequencies from 0 to 0.1. The airfoil was mounted between the sidewalls of the NASA Ames Research Center Fluid Mechanics Laboratory 25 cm \times 35 cm Compressible Dynamic Stall Facility (CDSF) and oscillated at $\alpha(t) = 10 \text{ deg} - 10 \text{ deg} \sin \omega t$. The freestream turbulence intensity in this in-draft facility has been reported by Davis⁸ to be 0.083% at 58 m/s, with a bandwidth of 50 Hz to 50 KHz. Reference 9 provides a complete description of the CDSF and its instrumentation.

One-hundred-forty-eight closely spaced hot-film gauges were distributed over the surface of an oscillating, 15.24-cm chord NACA 0012 airfoil. The leading edge from $x/c = 0.1$ on the lower surface to $x/c = 0.25$ on the upper surface was covered with sensors at a pitch of 16 gauges/cm. Sets of four gauges (with the same pitch) were mounted over the rest of the upper surface at every 5% chord. The sensors were fabricated and installed on the airfoil by NASA Langley Research Center. All sensors were operated at an overheat ratio of 1.5. The gauges were connected to a bank of TSI Model

Presented as Paper 2002-0291 at the AIAA 40th Aerospace Sciences Meeting, Reno, NV, 14–17 January 2002; received 5 June 2002; revision received 30 October 2002; accepted for publication 25 November 2002. This material is declared a work of the U.S. Government and is not subject to copyright protection in the United States. Copies of this paper may be made for personal or internal use, on condition that the copier pay the \$10.00 per-copy fee to the Copyright Clearance Center, Inc., 222 Rosewood Drive, Danvers, MA 01923; include the code 0001-1452/03 \$10.00 in correspondence with the CCC.

*Research Professor and Associate Director, Navy–NASA Joint Institute of Aerospace Sciences, Department of Aeronautics and Astronautics; mailing address: NASA Ames Research Center, M.S. 260-1, Moffett Field, CA 94035-1000. Associate Fellow AIAA.

†Research Scientist, Mail Stop 230-2. Member AIAA.

1750/1755 anemometers. The anemometers were individually tuned for a bandwidth of about 6–8 KHz using the usual square wave test. At any time only 16 gauges were used. A calculation of the net heat addition to the boundary layer indicated that less than 100 mJ energy was added when all 16 sensors were operated together at this overheat ratio. Part of this total heat also is conducted away through the substrate. Because the heat added was a minute fraction of the total enthalpy of the boundary-layer fluid, it was concluded that no significant effects (such as heat tripping) were introduced into the flow. Data to be presented later show that the boundary layer was indeed laminar at low angles of attack, especially near the trailing edge where natural transition first starts, confirming this conclusion.

Analog outputs from the 16 hot-film gauges were simultaneously sampled along with the digital data of the airfoil angle-of-attack encoder using Microstar Laboratories, Inc., analog-to-digital converter and digital I/O boards. Sampling rates between 10 and 40 KHz were used, for a total of 40,000–80,000 samples/channel with the airfoil oscillating at frequencies of up to 22 Hz. These large sample sets were used for ensemble averaging by binning over one encoder count (< 1 -deg phase angle), which corresponds to an angle of attack of 0.08 deg or less. For all cases an adequate number of samples (40–100) were available in each bin. The data were analyzed primarily using the ensemble-averaged mean value of the hot-film gauge output voltages. In the data that are presented, the deviations from the cycle mean value at each phase angle are plotted. The cycle mean was calculated for all of the samples from a sensor as an arithmetic mean and then subtracted from the individual samples to eliminate the effects of varying dc offset and noise from the data sets being compared. The plotted voltages provide a qualitative estimate of the local ensemble-averaged surface shear stress on an arbitrary scale because of a lack of a calibration method for the unsteady shear stress in adverse-pressure-gradient flows.

In addition, comparisons with interferograms obtained in earlier research on this problem will be made where needed to confirm the various flow features that were observed in this study. This is particularly important because, without a direct calibration, the only features present in the signal are either a rise or fall in the heat-flux values. The meaning is clear in some instances, such as transition onset, but it needs to be studied in the context of the local flow for each condition to properly establish the flow physics.

The experiments were conducted for the following conditions: Mach number M , 0.2–0.45; reduced frequency $k = \pi f c / U_\infty$, 0–0.1 for $M = 0.2$ and 0.3, 0–0.05 for $M = 0.4$ and 0.45; angle of attack α , 10 deg–10 deg $\sin \omega t$; and Reynolds number Re , 0.7×10^6 to 1.6×10^6 .

Results and Discussion

Interpretation of Heat-Flux Gauge Output Traces

Interpretation of these data is difficult because the gauges are not calibrated and because zero surface shear stress does not represent a separated flow condition in unsteady flows. However, prior physical insight into some details aids in this effort. For example, a gradual thickening of the boundary layer with increasing angle of attack causes the skin friction to decrease, and hence the gauge output decreases. Laminar-to-turbulent transition causes the familiar abrupt increase in the sensor output. A laminar separation bubble is usually seen as a rapid drop in the sensor output that follows a mild reduction in output while the laminar boundary layer thickens with increasing angle of attack. Passage of the dynamic-stall vortex over the airfoil upper surface leaves a trace that appears as a gradually elevated output rising toward the airfoil trailing edge as the angle of attack is increased, whereas flow reattachment shows the opposite behavior. Transition front movement appears as an increase in the output voltage, progressing toward the leading edge as the angle of attack is increased, whereas relaminarization manifests itself with an opposite behavior. Furthermore, in addition to using these physical insights, the heat-flux gauge data have also been interpreted using compressible dynamic-stall information generated using PDI, which is a global, quantitative, flowfield visualization technique.

With this background the results of the study are discussed next.

Flow Details at $M = 0.3$

Figure 1 shows three PDI images for $M = 0.3$ and $k = 0.05$, which are instantaneous quantitative flow documentations at $\alpha = 4, 8,$ and 13.5 deg. The fringes seen in the image are constant density contours. (See Ref. 1 for a more complete explanation of interpretation of PDI images.) The important flow features are indicated in the figure for future reference. Figure 2 presents the ensemble-averaged

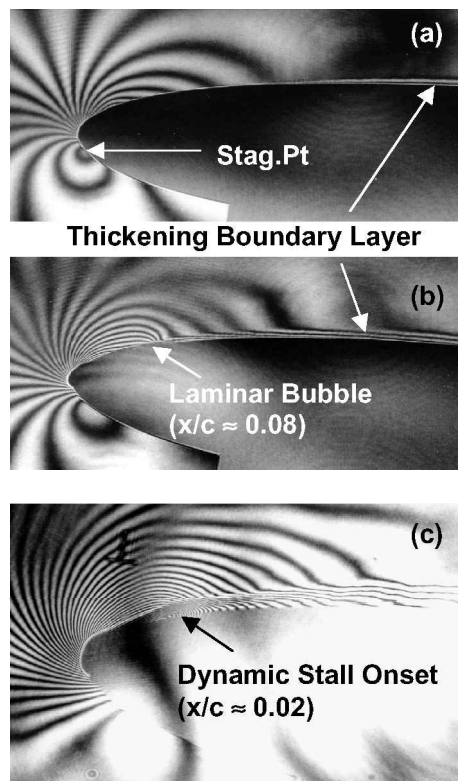


Fig. 1 PDI images of $M = 0.3$ and $k = 0.05$ flow: $\alpha =$ a) 4, b) 8, and c) 13.5 deg.

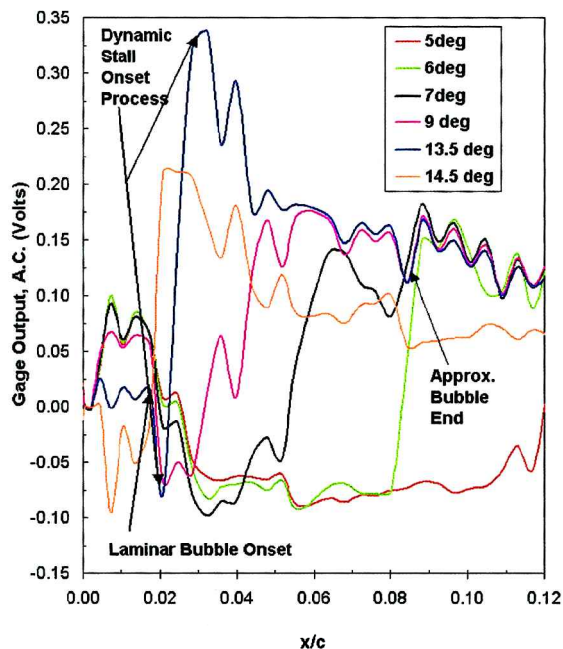


Fig. 2 Onset of dynamic stall from bubble bursting: $M = 0.3$ and $k = 0.05$.

gauge outputs in volts (obtained as just stated after subtracting the arithmetic cycle mean from all of the data for each sensor) for several angles of attack at $M = 0.3$ and $k = 0.05$. At low angles the flow is laminar over much of the upper surface. (See also discussion on transition behavior for both static and dynamic cases.) The trace for $\alpha = 5$ deg confirms that the shear stress is low over the range of x/c shown, but transition onset appears imminent beyond $x/c = 0.11$. At slightly higher angles a laminar separation bubble forms (see also Fig. 1b). When this occurs, the heat-flux gauge output falls rapidly, as seen at $x/c \approx 0.02$ for $\alpha = 6$ deg. At the end of the bubble, the surface shear stress increases abruptly over one sensor (at $x/c \approx 0.08$ in this case) because of the reattachment of the separated laminar shear layer as a turbulent boundary layer to close the bubble. The bubble is present until high angles of attack (13.5 deg). Over the sensors near the leading edge, the heat flux keeps falling, indicating that flow reversal is ongoing for all angles of attack for which the bubble remains on the airfoil. From the plots the onset location of the bubble is seen to be at $x/c \approx 0.018 - 0.02$, and the bubble appears to end at $x/c \approx 0.08$. This can be inferred from the fact that the shear-stress variations nearly coincide for $\alpha > 6$ deg here. (The cause of the waviness seen in these diagrams following the closure of the bubble is not known, but the amplitude of the waviness is within the standard deviation of the measurement locally, and, hence, it is believed to be insignificant.)

The conventional picture of the bubble containing a low energy recirculating fluid is supported by the very low shear-stress values near its upstream end. Where the bubble closes, there is an increase in the shear stress caused by the turbulent boundary layer at that location. However, because transition occurs in the free shear layer enveloping the bubble away from the surface, it cannot be detected in the surface-mounted gauge output, nor can it be detected in the PDI images because those are averaged over the airfoil span. Over locations within the bubble (see indicated region in Fig. 2), significant variations in the heat flux are measured, and the gauge output seems to increase over 8–10 sensors (see data for $\alpha = 7-9$ deg). It is now believed that this rise represents the footprint of some violent activity (probably attributable to a progressively strengthening reversed flow) that is initiated near the downstream end of the bubble and moves upstream with increasing angle of attack. Eventually, for $\alpha > 12$ deg (not shown) this evolves into a steep rise at $x/c = 0.02$ just after the bubble formation location. The steepness of this increase attains a maximum value at $\alpha = 13.5$ deg, where all of the change is seen over only one sensor and dynamic-stall onset ensues. The dynamic-stall onset event is seen clearly in Fig. 1c at the same x/c location and angle of attack. It is clear that the sharp rise corresponds to a dramatic increase in the local shear stress and implies a singular flow event driving the local flow. It has been deduced from the earlier PDI studies¹ that at $M = 0.3$ and $k = 0.05$ dynamic-stall onset occurs from the bursting of the laminar bubble and the present heat-flux gauge data clearly support that observation. It is intriguing to see such increasingly violent activity inside the bubble moving upstream when the angle of attack is increased, especially because the fluid contained in the bubble is deemed to be of low energy. Somehow, the fluid acquires the necessary energy to force itself upstream toward increasing pressure and cause an outburst from the leading edge of the bubble that induces a bubble-bursting type of dynamic stall. In computational studies Cui and Knight¹⁰ suggest a similar flow description. Subsequent to this event, the shear-stress level falls ($\alpha = 14.5$ deg) as the vortex convects past the upper surface.

Figure 3 shows the details of the surface flow recorded using the sensors on the upper surface across the bubble region as the airfoil was pitched up for $M = 0.3$ and $k = 0.1$. (In all of the color images that follow, red represents the highest sensor output and blue the lowest, with green at the middle of the scale corresponding to the cycle mean value.) These data are like those in Fig. 2 for $M = 0.3$ and $k = 0.05$, except that all traces are shown in the form of a continuous surface, whereas in Fig. 2 only six traces were shown. The various features just discussed are also present for the higher reduced frequency, and it is clear that dynamic stall arises from the leading end of the bubble as it bursts. Another new result

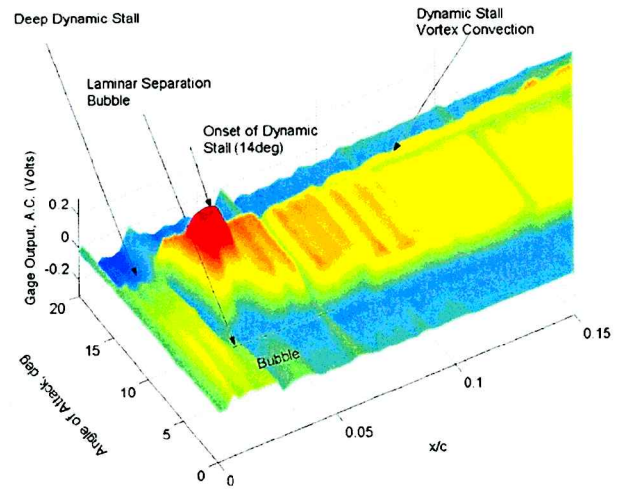


Fig. 3 Details of flow in the laminar bubble: $M = 0.3$ and $k = 0.1$.

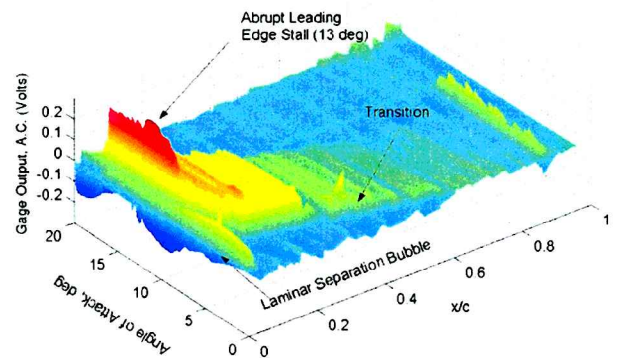


Fig. 4 Surface shear stress at $M = 0.3$ and $k = 0.001$.

of value here is the fact that, as the vortex grows and convects, the surface shear stress under it does not drop to zero or to a value where the fluid velocities are low (like in a typical dead-air region). The turbulence associated with the vortex and the flow on the backside of the vortex results in fairly large shear-stress levels during its passage. At any location the level falls off rapidly once the vortex passes. In the deep-stall phase the values on the upstroke are very small as indicated by the deep blue colors in the figure. Schreck et al.^{4,5} report similar results for incompressible dynamic-stall flow over a ramp-type pitching NACA 0015 airfoil at low Reynolds numbers.

Figure 4, which shows the full upper-surface flowfield for the steady/quasi-steady case at $M = 0.3$ (obtained by slowly oscillating the airfoil at $k = 0.001$), is presented in order to establish a basis for the surface-flow behavior studies for the unsteady cases. As in completely steady flow, the airfoil experiences abrupt leading-edge stall at the static-stall angle of attack, without the formation of a dynamic-stall vortex. The steady/quasi-steady stall arises from the bursting of the laminar separation bubble. Following this, the flow completely separates from the surface, and extremely low shear-stress values are seen. Even then, the unsteadiness in the shear layer can cause some intermittent reattachment just around the leading edge, and, hence, occasionally high shear-stress values are seen locally past the static-stall angle.

Figure 5, drawn for the case $M = 0.3$ and $k = 0.1$, clearly shows the convection of the dynamic-stall vortex for this unsteady case. This is in fact the major difference between Figs. 4 and 5. The vortex forms at $\alpha = 15$ deg, moves over the airfoil as indicated, and is still seen on the surface for $\alpha = 17$ deg. As stated in the Interpretation of Heat-Flux Gauge Output Traces section, the shear-stress ridge moves toward higher angles of attack as the vortex convects downstream. Prior to arriving at a downstream station, the

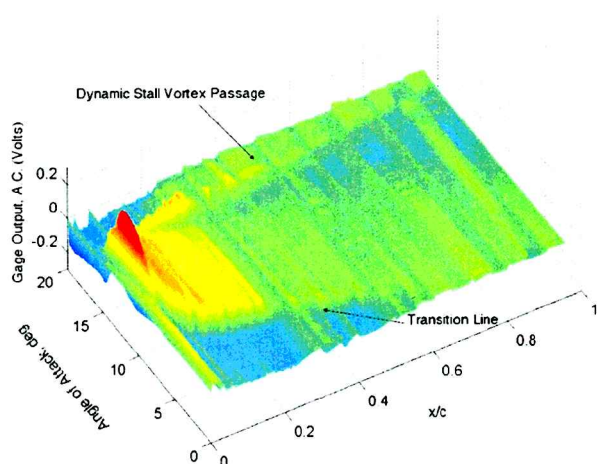


Fig. 5 Surface shear stress at $M = 0.3$ and $k = 0.1$.

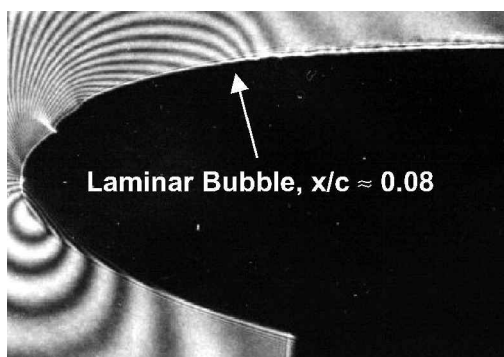


Fig. 6 PDI image for $M = 0.45$, $k = 0.05$, and $\alpha = 6.95$ deg.

blue region over the surface in Fig. 5 suggests that a dead-air region is present, possibly also indicating the upstream progression of a reversed flow region from the trailing edge.

Flow Details at $M = 0.45$ and $k = 0.05$

Figure 6 shows the PDI image at $M = 0.45$ for $\alpha = 6.9$ deg. At this condition the flow everywhere is subsonic, and the only major flow feature is the laminar separation bubble that was typical in all cases. However, as the airfoil pitches up, for example, by $\alpha = 9.5$ deg, shocks form in the flow. These are a series of shock waves and expansion waves that have been explained as transonic flow interactions.¹ Figure 7 shows a PDI image for this condition. The first shock is seen slightly ahead of the bubble origin, and the others ride on top of the shear layer enveloping the bubble. Reference 1 discusses the dynamic-stall onset mechanism for this condition, which is primarily shock induced.

The heat-flux data for this flow condition at various angles of attack are shown in the lower half of Fig. 7 to the same horizontal scale as that of the PDI image. The bubble forms at a much earlier angle of attack of 5 deg, in comparison with $M = 0.3$ flow, and for $\alpha = 5$ –7 deg, the bubble closes at $x/c \approx 0.08$. At all angles shown, the activity in the bubble is low between $x/c = 0.02$ and 0.055. The distributions show slight waviness in the region ahead of the bubble onset location, but the trace for $\alpha = 9.5$ deg shows a decrease and is then flat. The PDI studies showed a shock to first form at $\alpha \approx 9$ deg. Because the static temperature rises across a shock wave, the heat transfer from a heat-flux gauge at this location drops. Similarly, across an expansion wave the heat transfer rises. If the boundary layer near the leading edge where the shock forms is very thin ($\approx 100 \mu\text{m}$), the imprint of the shock can be picked up in the surface heat-flux traces. However, the same cannot be generally seen on sensors within the bubble. Interestingly, however, as the angle of attack increases the shock strength also increases, and as shown in Fig. 7 its imprint becomes visible even after the dynamic-stall

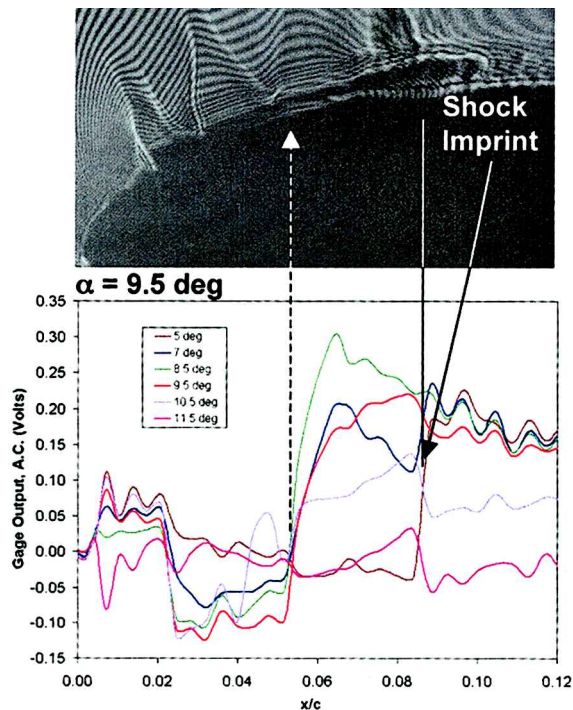


Fig. 7 Comparison of PDI at $\alpha = 9.5$ deg and heat-flux gauge data: $M = 0.45$ and $k = 0.05$.

onset has begun. Here the gauge output over $x/c = 0.084$ –0.088 (which corresponds to one sensor) decreases sharply for several angles. In Fig. 7 the shock-induced dynamic-stall onset point that is at $x/c = 0.055$ is also shown. At this point, once again, the shear stress rises abruptly (over only one sensor). The gradients involved are very high, as just discussed, and are comparable to those seen for $M = 0.3$. Beyond $\alpha = 12.5$ deg, shock-induced dynamic stall occurs. It is believed that dynamic-stall origination in the middle of the bubble is caused by the shock effects on the local recirculating flow region. In this flow a weak shear layer envelops the bubble and on top of that rides a strong series of shocks. The events that normally occur inside the bubble for nonshock flow conditions appear to be accelerated, and thus, dynamic stall occurs at a lower angle of attack at $M = 0.45$ compared to that at $M = 0.3$. Also, dynamic stall originates from the separation induced by these shocks and not by bubble bursting as was seen for $M = 0.3$ (as discussed in Ref. 1).

Behavior of Transition

The compressible dynamic-stall flow involves large changes in angle of attack and at model rotor Reynolds numbers (at which these tests were carried out); the airfoil boundary layer experiences transition and relaminarization during each cycle. Lack of appropriate understanding of these processes has been the key limitation on proper computational modeling of this flow. In particular, a unified model that accounts for the effect of Mach number and reduced frequency on the transition onset location as a function of angle of attack is crucial for this effort. It is hoped that results presented next will aid in this because transition onset location has been determined sufficiently accurately by using the rising heat-flux values. Generally, the rise in heat flux caused by transition is also preceded by gradually falling heat-flux values caused by the thickening of the laminar boundary layer. By individually plotting the ensemble-averaged gauge outputs measured in these experiments, it became possible to determine both the effect of Mach number and the effect of reduced frequency on transition behavior. These results provide the first recordings of the rapid upstream movement of the transition point in unsteady flow at model rotor conditions.

Figure 8a shows the Mach-number effect on transition movement at $k = 0.05$. It is seen that transition is accelerated when Mach number is increased (an effect partly caused by the increasing Reynolds

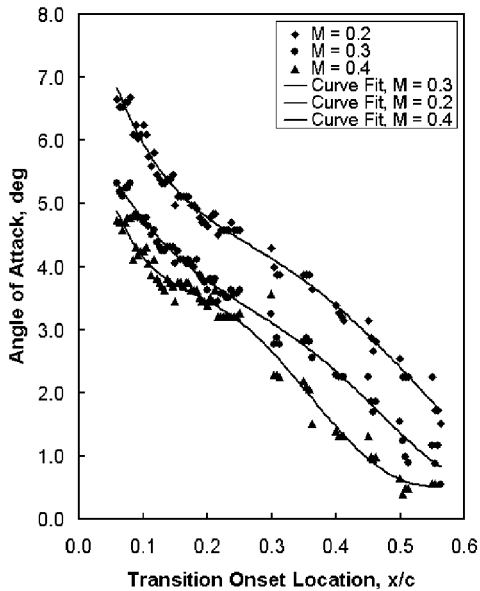


Fig. 8a Effect of Mach number on transition behavior: $k = 0.05$.

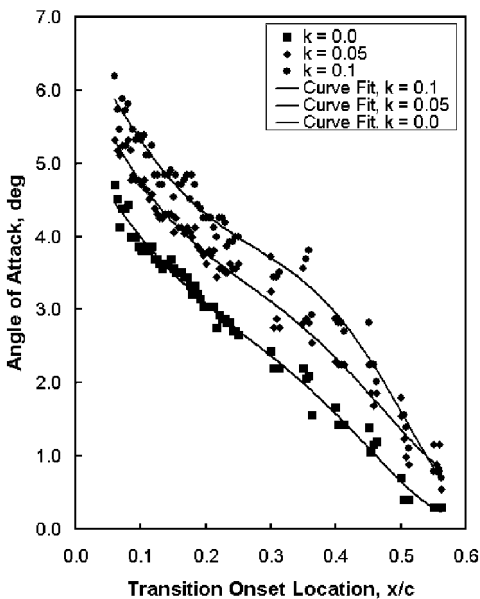


Fig. 8b Effect of reduced frequency on transition behavior: $M = 0.3$.

number associated with increasing the tunnel velocity at atmospheric conditions). Very low levels of heat flux result in a greater uncertainty in the effect beyond $x/c = 0.7$ ($\alpha < 0.5$ deg). But it is clear that transition starts near the trailing edge at very low angles of attack ($x/c = 0.6$, $\alpha = 0.5$ deg for $M = 0.4$, or $x/c = 0.6$, $\alpha \approx 1$ deg for $M = 0.3$) and moves rapidly upstream. The behavior becomes increasingly nonlinear (see the polynomial curve fit to the data) as the angle of attack increases, with an x/c movement of nearly 0.1 from $\alpha = 3-4$ deg for $M = 0.4$. Once the laminar bubble forms, transition occurs in the shear layer enveloping it and can no longer be seen in the heat flux signature.

Figure 8b shows the effect of reduced frequency at $M = 0.3$. Here, it is clear that transition onset is progressively delayed by increasing the degree of unsteadiness k , with a similar nonlinear behavior prevailing. However, the nonlinearity appears to increase slightly with frequency. This trend is consistent with that reported for studies by Schreck et al.⁴ and Kiedaisch and Acharya,² both of which were limited to incompressible flows over a ramp-type pitching airfoil.

Most dynamic-stall computations have hitherto been either fully turbulent or fully laminar, with very few exceptions (for example,

Ref. 11). Even in Ref. 11, the transition onset has been fixed for the most part to be very near the suction peak location. The results of the current study suggest that it is important to incorporate this new information on the transition behavior and the eventual relaminarization during each cycle (see the next section) for a more complete computational fluid dynamics (CFD) analysis.

Reattachment of Dynamic-Stall Flow

Figures 9a and 9b show the reattachment of the deep dynamic-stall flow on the downstroke for two cases. Figure 9a shows the results for the conditions of $M = 0.2$ and $k = 0.1$. The separated shear layer is highly turbulent and unsteady, but its surface imprint is basically void in heat transfer. The void in the heat flux remains for much of the deep-stall phase until the airfoil is at around 12 deg on the downstroke when the flow begins to reattach. This process starts from the leading edge as a turbulent process and proceeds in a systematic way, as indicated in Fig. 9a. When the airfoil angle of attack has decreased substantially, the boundary layer near the leading edge begins to relaminarize as the reattachment process continues. Eventually, at very low angles of attack ≈ 1 deg the entire flow becomes laminar, as seen in Fig. 9a. A laminar bubble also forms during this process,¹² as shown in the figure.

Similarly, for $M = 0.45$ and $k = 0.05$ the deep-stall flow has very little surface shear stress (blue regions in the figure), but around $\alpha = 10$ deg the shear layer begins to reattach. The higher Reynolds number of the flow results in higher local shear stress during reattachment, and relaminarization takes place in this case at even lower angles. It thus seems that, even though the dynamic-stall onset mechanism for the higher Mach number case is different, the reattachment process is largely similar, with only some differences in the angles at which the various events occur.

These details provide a clear documentation of the large changes in the transition and the surface shear stress that occur in this

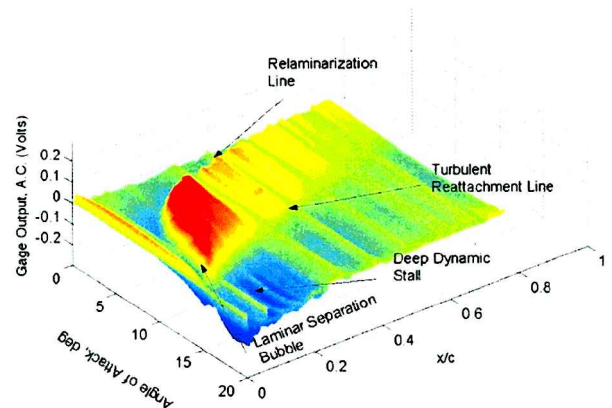


Fig. 9a Reattachment of dynamic-stall flow: $M = 0.2$ and $k = 0.1$.

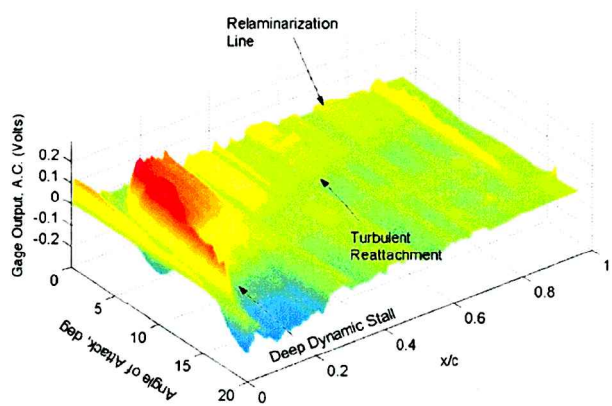


Fig. 9b Reattachment of dynamic-stall flow: $M = 0.45$ and $k = 0.05$.

complex flow. Incorporation of these new results in future CFD analysis of the flow might lead to a better agreement with experimental data.

Conclusions

The complex surface-flow physics of compressible dynamic stall has been experimentally documented using flush-mounted heat-flux gauges. The study has revealed the various surface-flow features and their changes under different flow conditions. It has also provided a description of the surface-flow events that lead to compressible dynamic-stall onset. The imprint of a leading-edge shock has been recorded for the first time in the surface-flow signature.

The dominant features of the flow are 1) the rapid movement over the airfoil of the transition point in the unsteady flow on the upstroke and flow relaminarization on the downstroke; 2) the formation of the dynamic-stall vortex at the leading edge through the bursting of the laminar separation bubble, or, at higher Mach numbers, through shock-induced flow separation from somewhere in the middle of the bubble; and 3) an extremely rapid rise of the surface shear stress at the onset of stall for different onset mechanisms.

A major conclusion reached from the study is that development of extremely large positive wall shear-stress gradients is a clear precursor to compressible dynamic-stall onset. It also appears to be the singular event that drives the flow into the stalled state, doing so for the widely varying dynamic-stall onset mechanisms that prevail for different flow conditions. Hence, it is expected that the same indicator will also serve as a precursor to full-scale rotor dynamic stall, even though a laminar bubble is unlikely to be present in the higher-Reynolds-number rotor case and some of the flow details will be different. A definitive result can be obtained by repeating the present studies on a tripped airfoil. The information generated here can be used to develop suitable transition and relaminarization models to be included in the computational studies of the flow for more realistic results.

Acknowledgments

This work was supported by Army Research Office under Grant MIPR0KKNPGAS052 to the U.S. Naval Postgraduate School, Monterey, California, and monitored by T. L. Doligalski. The heat-flux gauge sensors on the airfoil were installed at NASA Langley Research Center, Hampton, Virginia, with design help from J. L. Bartlett. The TSI anemometers were made permanently available to this research from the U.S. Air Force Academy, Colorado Springs,

Colorado, and the assistance of S. J. Schreck in this regard is sincerely appreciated. The discussions with L. W. Carr and S. S. Davis and the support of the NASA Ames Fluid Mechanics Laboratory staff are gratefully acknowledged.

References

- ¹Chandrasekhara, M. S., Wilder, M. C., and Carr, L. W., "Competing Mechanisms of Compressible Dynamic Stall," *AIAA Journal*, Vol. 36, No. 3, 1998, pp. 387–393.
- ²Kiedaisch, J. W., and Acharya, M., "Investigation of Incipient Dynamic Stall over Pitching Airfoils Using Hot-Film Sensors," AIAA Paper 97-0656, Jan. 1997.
- ³Lee, T., and Basu, S., "Measurement of Unsteady Boundary Layer Developed on an Oscillating Airfoil Using Multiple Hot-Film Sensors," *Experiments in Fluids*, Vol. 25, No. 1, 1998, pp. 108–117.
- ⁴Schreck, S. J., Faller, W. E., and Helin, H. E., "Pitch Rate and Reynolds Number Effects on Unsteady Boundary Layer Transition and Separation," *Journal of Aircraft*, Vol. 35, No. 1, 1998, pp. 46–52.
- ⁵Schreck, S. J., Faller, W. E., and Robinson, M. C., "Unsteady Separation Processes and Leading Edge Vortex Precursors: Pitch Rate and Reynolds Number Influences," AIAA Paper 2000-2605, June 2000.
- ⁶Nakayama, A., Stack, J. P., Lin, J. C., and Valarezo, W. O., "Surface Hot-Film Technique for Measurements of Transition, Separation, and Reattachment Points," AIAA Paper 93-2918, July 1993.
- ⁷Stack, J. P., Mangalam, S. M., and Berry, S. A., "A Unique Measurement Technique to Study Laminar-Separation Bubble Characteristics on an Airfoil," AIAA Paper 87-1271, June 1987.
- ⁸Davis, S. S., "Measurement of Discrete Vortex Noise in a Closed Throat Wind Tunnel," AIAA Paper 75-488, March 1975.
- ⁹Carr, L. W., and Chandrasekhara, M. S., "Design and Development of a Compressible Dynamic Stall Facility," *Journal of Aircraft*, Vol. 29, No. 3, 1992, pp. 314–318.
- ¹⁰Cui, A., and Knight, D. D., "Parallel Computation of the 2-D Navier–Stokes Flowfield of a Pitching Airfoil," *Computational Fluid Dynamics*, Vol. 4, 1995, pp. 111–135.
- ¹¹Geissler, W., Carr, L. W., Chandrasekhara, M. S., Wilder, M. C., and Sobieczky, H., "Compressible Dynamic Stall Calculations Incorporating Transition Modeling for Variable Geometry Airfoils," AIAA Paper 98-0705, Jan. 1998.
- ¹²Ahmed, S., and Chandrasekhara, M. S., "Reattachment Studies of an Oscillating Airfoil Dynamic Stall Flow Field," *AIAA Journal*, Vol. 32, No. 5, 1994, pp. 1006–1012; also AIAA Paper 91-3225, 1991.

A. Plotkin
Associate Editor

Color reproductions courtesy of the Naval Postgraduate School.